Wang et al. SpringerPlus (2016) 5:369
DOI 10.1186/s40064-016-1805-5

SpringerPlus

RESEARCH Open Access

MO degradation by Ag–Ag_2O/g-C_3N_4 composites under visible-light irradiation

Xin Wang[1], Jia Yan[1], Haiyan Ji[1], Zhigang Chen[1], Yuanguo Xu[1], Liying Huang[1], Qi Zhang[2], Yanhua Song[3], Hui Xu[1*] and Huaming Li[1*]

*Correspondence: xh@ujs.edu.cn; lihm@ujs.edu.cn
[1] School of Chemistry and Chemical Engineering, Institute for Energy Research, Jiangsu University, Zhenjiang 212013, People's Republic of China
Full list of author information is available at the end of the article

Abstract

The paper demonstrated the synthesis of Ag–Ag_2O/g-C_3N_4 nanoparticles via a simple liquid phase synthesis path and a facile calcination method. The synthesized Ag–Ag_2O/g-C_3N_4 composites were well characterized by various analytical techniques, such as X-ray diffraction, Fourier transform infrared (FT-IR), X-ray photoemission spectroscopy, transmission electron microscopy, scanning electron microscopy, high resolution transmission electron microscopy, the UV–Vis diffuse-reflectance spectra and transient photocurrent. From the structure and surface characterization, it indicated that Ag–Ag_2O/g-C_3N_4 composites were formed by an effective covering of g-C_3N_4 with Ag–Ag_2O. The results revealed that the 50 wt% nanoparticle had a great effection on the degradation of the methyl orange (MO), which was almost 7.5 times as high as that of g-C_3N_4. Based on the experimental results, the possible photocatalytic mechanism with photogenerated holes as the main active species was presented.

Keywords: Ag–Ag_2O, g-C_3N_4, MO, Photocatalytic

Background

With the development of the society, the environmental pollution has become one of the important problems which aroused more and more focus. It is well known that the TiO_2 has been proved to be the most distinguished and widely used in the photocatalytic degradation of dyes (Liu et al. 2008; Chang et al. 2014) and H_2 production (Cho et al. 2011; Park et al. 2006; Yang et al. 2009). However, with the increasing demands of the photocatalytic materials searching for more semiconductor photocatalysts is becoming more urgent. Thus, the mental and non-mental composites with g-C_3N_4 have attracted more attention (Peng et al. 2013; Zong et al. 2013).

As a good photocatalyst, Graphitic carbon nitride (g-C_3N_4) has been widely investigated since the discovery of its excellent properties by Liu and Cohen (1989). To date, it exhibits catalytic activity for extensive reactions, such as water splitting, oxidation reaction, dye photodegradation, nitric oxide (NO) decomposition and so on (Huang et al. 2013; Vignesh and Kang 2015; Chen et al. 2015; Yu et al. 2015; Dong et al. 2015; Chang et al. 2013; Su et al. 2010). This new material also possesses the good capabilities such as environmental friendly, stable, low cost and efficient. The reason why the g-C_3N_4 has a good photocatalytic activity is that the g-C_3N_4 possesses special optical characteristics and outstanding chemical stability. But, even with those merits, the g-C_3N_4 still has

some disadvantages which show the limited photocatalytic property, such as the poor dispersion, easy agglomeration, recycling difficulties and so on. Yet combined with other materials such as the g-C_3N_4/MoO_3 (Huang et al. 2013), g-C_3N_4/Ni(dmgH)$_2$ (Cao et al. 2014), g-C_3N_4/$Bi_2O_2CO_3$ (Tian et al. 2014), g-C_3N_4/Ag_3PO_4 (Xiu et al. 2014) and so on could enhance the catalytic activity of g-C_3N_4.

For example, in recent years, a g-C_3N_4 was modified with a composite semiconductor could possess the performance of water splitting and remove organic pollutants, which were reported by Wang et al. (2009) and Zhao et al. (2012). Wang and Zhang (2012) reported a g-C_3N_4–TiO_2 pohotocatalyst fabricated by a simple impregnation method which has good activities for the H_2 production. In fact, the approach indicates a synergetic effect of the impregnation preparation which provides a better junction between g-C_3N_4 and TiO_2. It can be seen that the composites may have better photoactivities. However, not only can TiO_2 doped possess the properties of degrading the pollutants, but also other mental and non-mental materials doped could have good activities. As we all know, the Ag-based materials have good photocatalytic activity. Thus, enormous efforts have been made to study more photocatalysts which needed Ag-based materials modification, such as Ag/C_3N_4 (Li et al. 2015), Ag/$AgVO_3$/g-C_3N_4 (Zhao et al. 2015), Ag/AgCl/g-C_3N_4 (Yao et al. 2014), Ag–AgBr/g-C_3N_4 (Li et al. 2014) and so on.

In this paper, the Ag–Ag_2O/g-C_3N_4 composites were successfully fabricated via a simple liquid phase synthesis path and a facile calcination method. The approach is different from the paper that has been reported by Xu et al. (2013) and Ren et al. (2014). The preparation of Ag–Ag_2O can be described as following (Yu et al. 2014):

$$2AgNO_3 + Na_2CO_3 \rightarrow Ag_2CO_3 \downarrow + 2NaNO_3 \quad (1)$$

$$Ag_2CO_3 \rightarrow Ag_2O + CO_2 \uparrow \quad (2)$$

$$2Ag_2O \rightarrow 4Ag + O_2 \uparrow \quad (3)$$

Simultaneously, Ag_2O nanoparticles were partially reduced to Ag^0 as it was calcined at 220 °C for 90 min to prepare the desired Ag–Ag_2O photocatalysts. This method is also used the same as the preparation of Ag–Ag_2O/g-C_3N_4 nanocomposites. Then the intimate contacted interfaces between the Ag–Ag_2O and g-C_3N_4 were also developed. In addition, prepared g-C_3N_4 via Ag–Ag_2O doping has been proved to control the migration photon-generated carriers, so that the electrons and holes could be separated selectively at the edges, respectively. The mechanism of this report can explain phenomenon for it which indicates Ag–Ag_2O has a great potential to be used as a stable and highly efficient photocatalyst to degrade the pollutants under the visible-light irradiation. MO, a representative of dyestuffs resistant to biodegradation, was selected as a model for the study. From our study, we find that the proportion of Ag–Ag_2O loading on g-C_3N_4 surface has the most enhanced adsorption capacity and the best photocatalytic activity is 50 wt%. Therefore, both Ag and Ag_2O maybe act as traps to capture photogenerated electrons which contribute to the separation of electron–hole pairs (Yu et al. 2005, 2012; Zhou et al. 2010; Subramanian et al. 2001; Xie et al. 2011). Based on the experimental results, a possible photocatalytic mechanism for the degradation of MO over Ag–Ag_2O doped g-C_3N_4 nanosheets under visible-light irradiation was proposed.

Experimental section

Materials

All reagents in this work were AR grade and used without further purification.

Preparation of g-C_3N_4

The g-C_3N_4 was synthesized by calcination method. In a typical process, 6 g dicyandiamide was put into three crucibles with three covers, sealed in a quartz tube partially backfilled with pure nitrogen, annealed at 350 °C for 2 h and annealed at 600 °C for 2 h again. Then the crucibles were cooled to room temperature.

Preparation of Ag–Ag_2O/g-C_3N_4 nanoparticles

The Ag–Ag_2O/g-C_3N_4 was also synthesized via a simple liquid phase synthesis path and a facile calcination method. The method was as follow: 0.2 g of g-C_3N_4 was added into 20 ml of deionized water. Then they were magetic stirred for 5 min and sonicated for 15 min. Further, 0.2932 g of silver nitrate ($AgNO_3$) was added into the solution and sonicated for 15 min. Next, 0.5 ml hydrated ammonia ($NH_3{\cdot}H_2O$) was also added into the solution, which was still magetic stirred for 15 min. In addition, 0.1829 g of sodium carbonate (Na_2CO_3) was added drop by drop under stirring in 15 min. Moreover, the pH of the solution was adjusted to 7 and heated in water bath at 25 °C for 1 h. Next, the product was obtained by centrifugation, washed with ethanol and deionized water for several times and dried at 60 °C for 8 h. At last, the sample was annealed at 220 °C for 90 min. The 50 wt% Ag–Ag_2O/g-C_3N_4 could be obtained. All the experiments were carried out at room temperature. The Ag–Ag_2O/g-C_3N_4 composites with different mass ratios were synthesized using the same method through changing the amount of g-C_3N_4, $AgNO_3$ and Na_2CO_3, such as 5, 10, 30 and 40 wt%, respectively.

Characterization

The crystal phase of Ag–Ag_2O, g-C_3N_4 and Ag–Ag_2O/g-C_3N_4 powders were analyzed by X-ray diffraction (XRD) analysis using a Bruker D8 diffractometer with Cu-Kα radiation ($\lambda = 1.5418$ Å) in the 2θ range of 20°–80°. Scanning electron microscopy (SEM) image and transmission electron microscopy (TEM) micrographs were taken with a JEOL-JEM-2010 (JEOL, Japan) operating at 200 kV. High resolution transmission electron microscopy (HR-TEM) micrographs were taken with a FEI F20. Energy Dispersive spectrum (EDS) measurements were performed by a JEM-2100F electron microscope. The UV–Vis diffuse-reflectance spectra (DRS) of the samples were obtained on a UV–Vis spectrophotometer (UV-2450, Shimadzu Corporation, Japan). They were measured in solid state, and $BaSO_4$ powder was used as the substrate. Fourier transform infrared (FT-IR) spectra of all the catalysts (KBr pellets) were recorded on Nicolet Model Nexus 470 IR equipment. X-ray photoemission spectroscopy (XPS) was measured on a PHI5300 with a monochromatic Mg Kα source to explore the elements on the surface. The photocurrents were measured with an electrochemical analyzer (CHI660B, CHI Shanghai, Inc.).

Results and discussion

The XRD patterns of the as-prepared Ag–Ag_2O, g-C_3N_4 and Ag–Ag_2O/g-C_3N_4 composites were shown in Fig. 1. All diffraction peaks could be indexed as "★" of Ag, "◆" of Ag_2O, "●" of g-C_3N_4. The results indicated that the diffraction peak at 13.1° and 27.8° could be indexed as (100) and (002) diffraction planes (JCPDS 87-1526) (Wang et al. 2009). And the (100) diffraction peak is weakening with the decreasing content of g-C_3N_4. With the increasing Ag–Ag_2O content, the diffraction peaks at 32.8° and 54.9° gradually appeared while the intensity increased, and the peaks were assigned to the (111) and (220) planes (JCPD 41-1104) (Wang et al. 2011) of Ag_2O crystal, respectively. Four diffraction peaks at 32.8°, 44.3°, 64.4° and 77.5° in Ag were indexed to the (111), (200), (220) and (311) planes of Ag (JCPDS 04-0783) (Liu et al. 2015), respectively. As discussed above, the Ag–Ag_2O/g-C_3N_4 nanocomposites were successfully prepared via a simple liquid phase synthesis path and a facile calcination method.

Figure 2 showed the FTIR spectra of the Ag–Ag_2O, g-C_3N_4 and a series of Ag–Ag_2O/g-C_3N_4 composite photocatalysts, respectively. The broad peak at 3000–3500 cm^{-1} was ascribed to the stretching vibration of N–H and that of O–H of the physically adsorbed water (Xu et al. 2013; Yan et al. 2014). In the case of g-C_3N_4, the strong band of 1200–1700 cm^{-1}, with the characteristic peaks at 1242, 1322, 1412, 1563 and 1634 cm^{-1} were attributed to the typical stretching vibration of CN heterocycles (Xu et al. 2013; Yan et al. 2014). In addition, the peak at 807 cm^{-1} is associated with the breathing mode of triazine units (Min and Lu 2012; Lotsch and Schnick 2006). Moreover, for the Ag–Ag_2O, the observed broad peak around 600 cm^{-1} belongs to Ag–O bond vibration (Xu et al. 2013). The FT-IR spectra of the Ag–Ag_2O/g-C_3N_4 composites represented the spectra of both g-C_3N_4 and Ag–Ag_2O. It should be noted that the intensity of the peak at 807 cm^{-1} decreased with the reduction of the g-C_3N_4 content.

XPS was further made use of to analyze the chemical status and compositions of the 50 wt% Ag–Ag_2O/g-C_3N_4 composite. Figure 3a showed the XPS analysis spectrum of the as-prepared composites, from which only Ag, O, C and N elements could be observed. In order to investigate the detailed chemical states of 50 wt% Ag–Ag_2O/g-C_3N_4

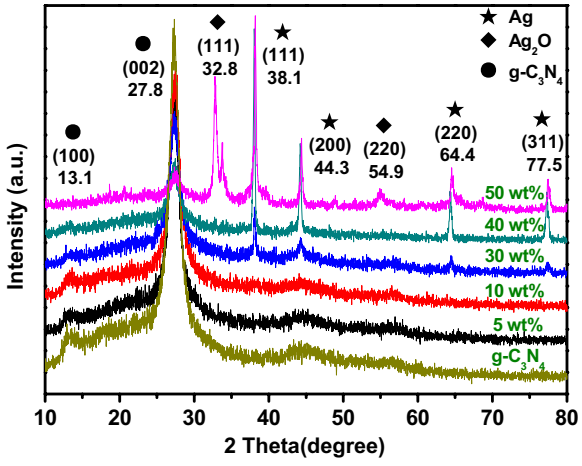

Fig. 1 XRD patterns of Ag–Ag_2O, g-C_3N_4 and Ag–Ag_2O/g-C_3N_4 composite

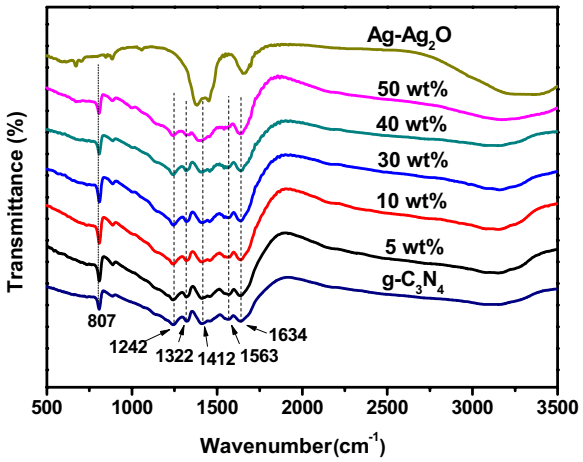

Fig. 2 FT-IR of the as synthesized Ag–Ag_2O, g-C_3N_4 and Ag–Ag_2O/g-C_3N_4 composite

nanoparticles, the peaks of Ag 3d, O 1s, C 1s and N 1s had been conducted and given in Fig. 3b–e. There were two peaks located at 374.2 and 368.2 eV could attach to the binding energies of $Ag3d_{5/2}$ and Ag $3d_{3/2}$ (Melian et al. 2012), which belonged to Ag^+ in Ag–Ag_2O (Fig. 3b). Besides, the peak at 368.2 eV could be further divided into two bands of 368.1 eV and 369.0 eV for the binding energy of Ag(I) $3d_{5/2}$ and Ag(0) $3d_{3/2}$, respectively. And the peak at 374.2 eV could be also de-convoluted into two different peaks at 374.1 eV and 374.9 eV for Ag(I) $3d_{5/2}$ and Ag(0) $3d_{3/2}$, respectively. The peak centered at 530.9 eV could be attributed to the lattice oxygen atoms of Ag–Ag_2O (Huang et al. 2013) (Fig. 3c). Figure 3d showed that the peaks located at 288.2 and 284.7 eV correspond to the sp^3-bonded C in C–N of g-C_3N_4 and C–C coordination of the surface adventitious carbon (Li et al. 2013; Yan et al. 2012; Yan et al. 2010). Compared with the intensity of g-C_3N_4, the peak at 288.2 eV was strengthened and the peak at 284.7 eV was weakened. In the N 1s spectrum (Fig. 3e), the peak at 398.8 eV was assigned to C=N–C coordination (Wang et al. 2014), the intensity of which was stronger than that of g-C_3N_4. In the N 1s spectrum (Fig. 3e), the peak at 398.8 eV was assigned to C=N–C coordination (Wang et al. 2014). In the end, results from XRD, FT-IR and XPS indicated that the as-prepared samples contained Ag–Ag_2O and g-C_3N_4.

The morphological characterization of as-synthesized products was investigated by using SEM and TEM. SEM images were shown in Fig. 4a, b, which clearly depicted layer structure of g-C_3N_4 (Xu et al. 2013). From SEM images, it was obvious that these Ag–Ag_2O nanoparticles were well dispersed on the surface of the g-C_3N_4. To further observe the combination of Ag–Ag_2O and g-C_3N_4, EDS mapping images were shown in Additional file 1: Fig. S1, which indicated that Ag and O element were well distributed in the samples. TEM was used to investigate the morphology and microstructure of the sample. The TEM and HR-TEM images of 50 wt% Ag–Ag_2O/g-C_3N_4 were shown in Fig. 4c–e. It can be seen that Ag–Ag_2O particles were uniformly deposited on the surface of g-C_3N_4. The existence of heterojunction between Ag and Ag_2O could be seen in the HR-TEM. Two different kinds of lattice fringes were clearly observed. The d = 0.236 of the first fringe matches the (111) crystallographic plane of Ag (Liu et al. 2015), and another

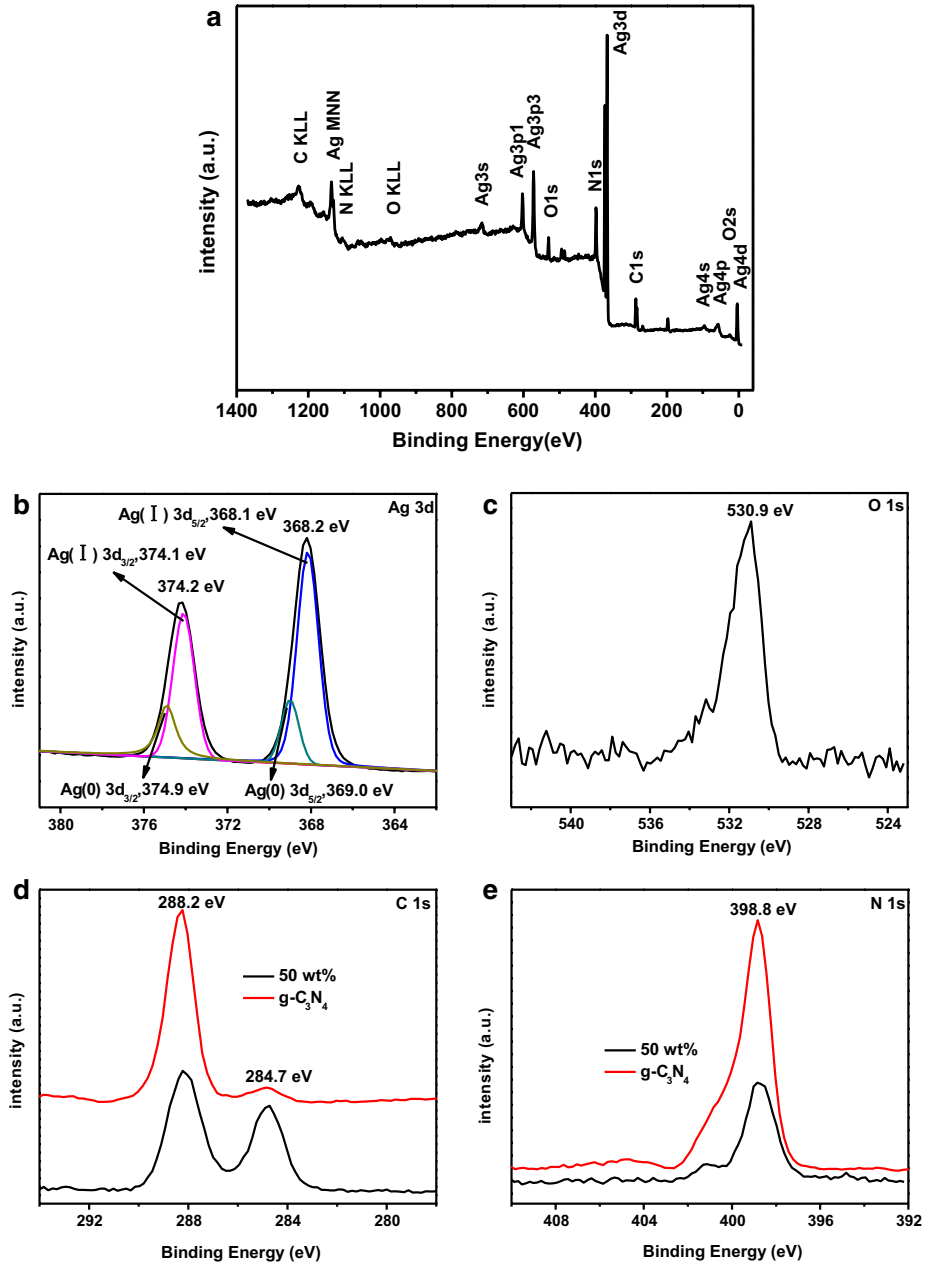

Fig. 3 XPS spectra **a** profiles of survey, **b** Ag 3d, **c** O 1s, **d** C 1s and **e** N 1s

of d = 0.273 and 0.167 nm are attached to the (111) and (220) crystallographic plane of Ag_2O (Wang et al. 2011) respectively. What's more, an integration interface between g-C_3N_4 and Ag–Ag_2O is possibly formed, which was contributed to the transport of photoexcited carriers. At last, from the EDS, we could see that there were only Ag, O, C, N and Si elements, which consistent with the XRD in Fig. 4f. The corresponding EDS spectrum of the sample 50 wt% Ag–Ag_2O/g-C_3N_4 confirmed that there were C, N, O, Si and Ag elements in the sample as shown in Fig. 4f. Also from the Additional file 1: Table

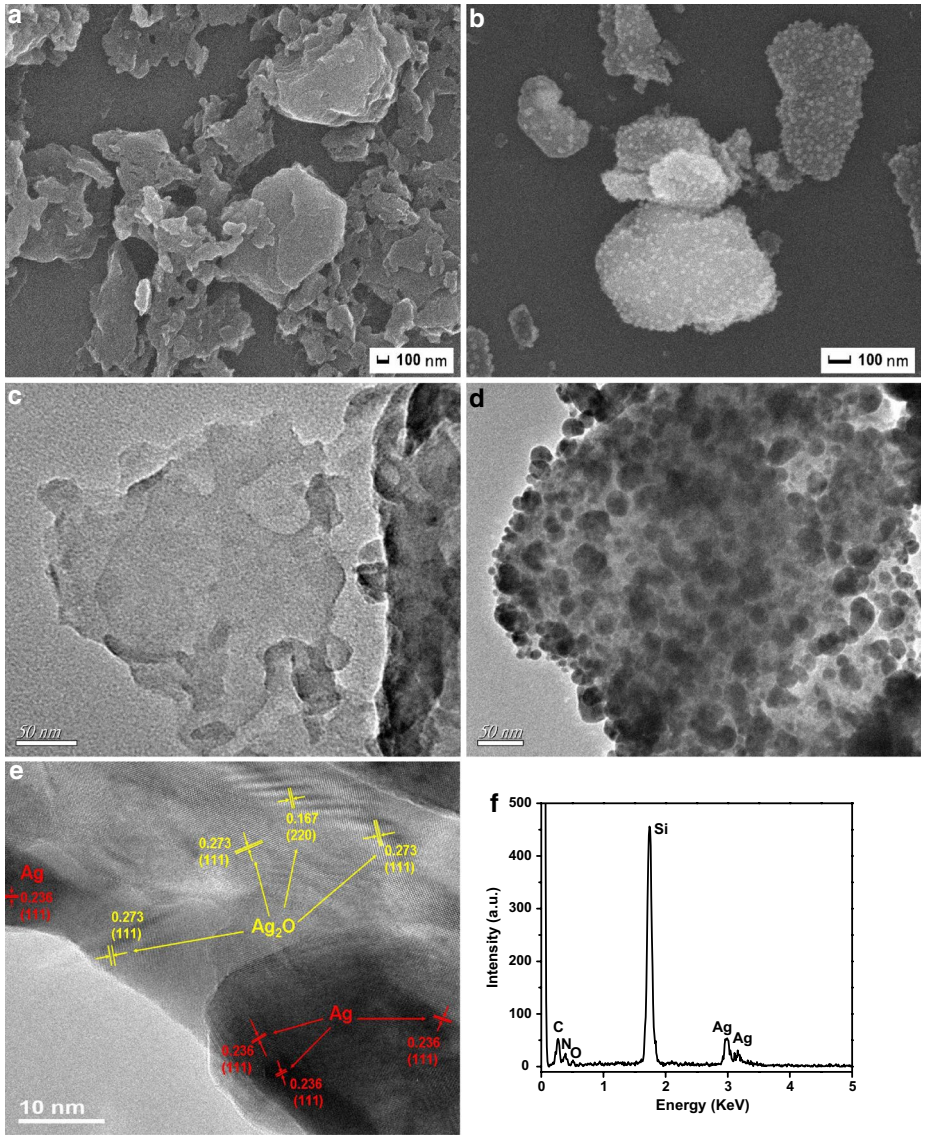

Fig. 4 SEM morphologies of g-C_3N_4 (**a**), 50 wt% Ag–Ag_2O/g-C_3N_4 (**b**), TEM morphologies of g-C_3N_4 (**c**), 50 wt% Ag–Ag_2O/g-C_3N_4 (**d**), HR-TEM morphologies of 50 wt% Ag–Ag_2O/g-C_3N_4 (**e**) and EDS of the 50 wt% Ag–Ag_2O/g-C_3N_4 composite (**f**)

S1, the actual data of the content of Ag–Ag_2O in the sample were close to the theoretical data of that. Even though there were some differences between the theoretical data and the actual data, these might be due to the loss of g-C_3N_4 in the calcination process. In addition, the observed Si peaks in the above EDS spectrum arose from the silicon grids was used for SEM analysis.

The DRS of Ag–Ag_2O/g-C_3N_4, Ag–Ag_2O and g-C_3N_4 were shown in Fig. 5. The absorption edges were varied by changing the amount of Ag–Ag_2O. As shown in Fig. 5a, the g-C_3N_4 had the absorption edge of around 460 nm. When the ratio of Ag–Ag_2O/g-C_3N_4 was increased from 5 to 50 wt%, the absorption edge of the composites shifted to the larger wavelength region and the composites exhibited stronger absorbance in the visible region

due to the surface plasmon resonance (SPR) absorption of metal Ag nanocrystal. Compared with the 30 wt% and 50 wt% Ag–Ag_2O/g-C_3N_4 composites, the 30 wt% Ag–Ag_2O/g-C_3N_4 showed more obvious SPR than 50 wt% Ag–Ag_2O/g-C_3N_4 which had more content of Ag–Ag_2O attached to the surface of g-C_3N_4, that leaded to the absorption peak widen and then changed the SPR (Xu et al. 2011). The band gap values (E_g) of Ag–Ag_2O and g-C_3N_4 were calculated by plots of $(\alpha h\upsilon)^{1/2}$ versus photon energy, which were shown in Fig. 5b. From the Fig. 5b, the band gap energy of g-C_3N_4 was 2.7 eV. At the same time, the band energy of Ag–Ag_2O was 1.3 eV, which would be used in the possible mechanism at the end. To give a direct analysis, the potentials of the conduction band (CB) and valence band (VB) edges of g-C_3N_4 and Ag_2O were evaluated by Mulliken electronegativity theory:

$$E_{CB} = X - E_C - 1/2E_g$$

$$E_{CB} = E_{VB} - E_g$$

where X was the absolute electronegativity of the atom semiconductor [$(X_{Ag2O} = 4.44 * 4.44 * 7.54)^{1/3} = 5.29$], defined as the geometric mean of the absolute electronegativity of the constituent atoms, and expressed as the arithmetic mean of the atomic

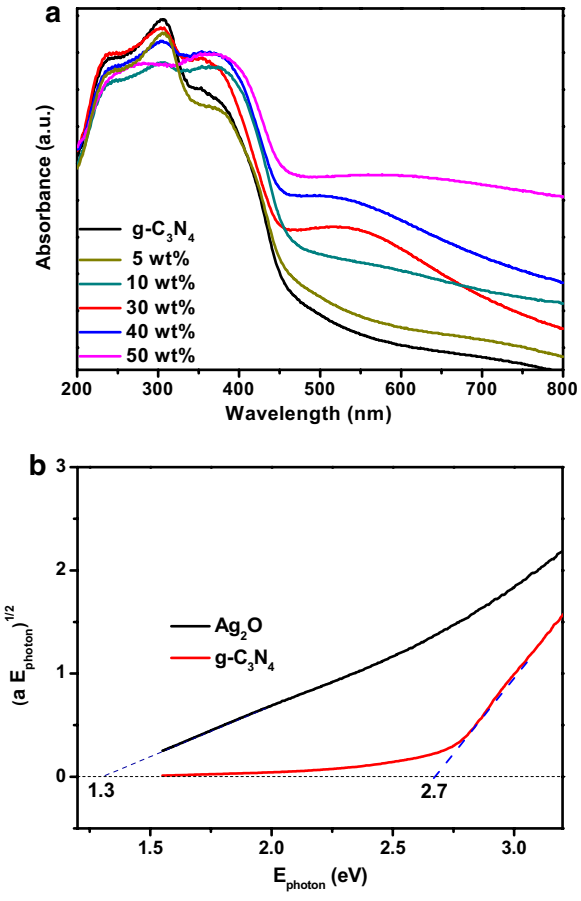

Fig. 5 DRS (**a**), versus photon energy of the Ag–Ag_2O/g-C_3N_4 treated for different proportions and plots of $(\alpha h\upsilon)^{1/2}$ (**b**) versus photon energy of the Ag_2O and g-C_3N_4

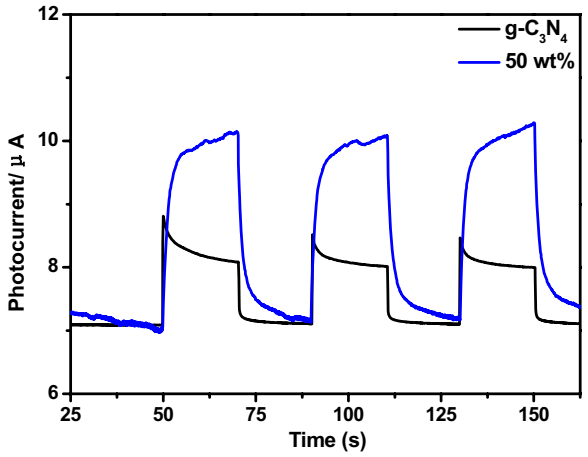

Fig. 6 Transient photocurrent response for g-C_3N_4 and 50 wt% Ag–Ag_2O/g-C_3N_4 composite

electro affinity and the first ionization energy; E_C was the energy of free electrons with the hydrogen scale (4.5 eV); E_g was the band gap of the semiconductor (Xu et al. 2013). Based on the band gap positions, the CB and VB edge potentials of Ag_2O were at +0.14 eV and +1.44 eV, respectively. The CB and VB edge potentials of g-C_3N_4 were at −1.13 eV and +1.57 eV, which were consistent with the previous literature, respectively (Xu et al. 2013).

Commonly, a high value of the photocurrent demonstrates that the composite holds strong ability in generating and transferring the photoexcited charge carrier under irradiation. As shown in Fig. 6, the g-C_3N_4 and different ratios of Ag–Ag_2O/g-C_3N_4 composite were characterized by transient photocurrent. The 50 wt% Ag–Ag_2O/g-C_3N_4 had a higher photocurrent than g-C_3N_4, which indicates that Ag–Ag_2O/g-C_3N_4 composite exhibits stronger ability than g-C_3N_4 in the separation of electron–hole pairs. While under visible-light irradiation, the pure g-C_3N_4 showed lower photocurrent response, because of its lower efficiency of the charge carriers' separation. The results in Fig. 6 could well correspond to those from the MO degradation experiments which were shown as the following.

Figure 7 showed the MO degradation curves of the photocatalysts of g-C_3N_4 and Ag–Ag_2O/g-C_3N_4 with different Ag–Ag_2O modifying amount under visible light irradiation. As shown in Fig. 7, the g-C_3N_4 showed poor activity, on which ~12 % of MO was decomposed after visible light irradiation for 3.5 h. After combining Ag–Ag_2O with g-C_3N_4, the experiments clearly demonstrated that the Ag–Ag_2O/g-C_3N_4 composite was determined as an efficient visible light photocatalyst, which was higher than the g-C_3N_4. Above all, the photoactivity of 50 wt% Ag–Ag_2O/g-C_3N_4 composite was about 7.5 times higher compared to g-C_3N_4 and had the best photoactivity of all. The results may according to that there is a heterojunction between the Ag–Ag_2O and g-C_3N_4, which can improve separation of electron–holes pairs and therefore enhance the photocatalytic activity of the g-C_3N_4.

Hydroxyl radicals and photogenerated holes are two main species for the oxidization of organic molecular in aqueous solution. In order to understand the photocatalysis

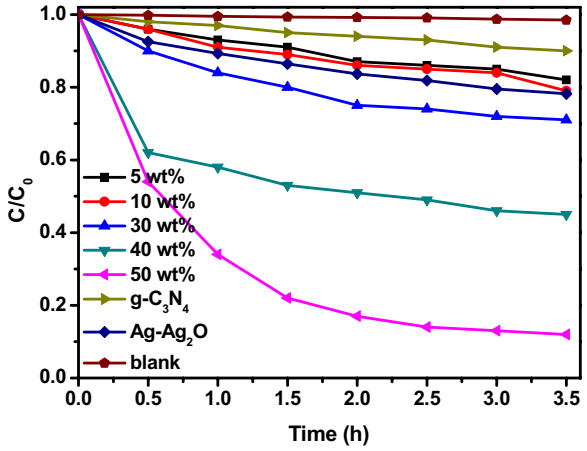

Fig. 7 MO dye degradation curves of the g-C_3N_4 and Ag–Ag_2O/g-C_3N_4 with different Ag–Ag_2O modifying amount under visible light irradiation

profoundly, the effects of holes and hydroxyl radicals on the photocatalytic evaluation were investigated. As shown in Fig. 8, due to the tert-Butyl alcohol (TBA) could efficiently entrap the ·OH radicals, which was selected as ·OH scavenger. The change for the photodegradation of MO was small of the TBA, revealing that the hydroxyl radicals were not the main active species. However, after introducing EDTA-2Na as a hole scavenger, the photodegradation efficiency of MO over Ag–Ag_2O/g-C_3N_4 greatly reduced from 95 to 11 % after irradiation for 4.5 h. These results indicated that the holes played an important role in the degradation of MO over Ag–Ag_2O/g-C_3N_4.

The Fig. 9 showed the possible mechanism of photodegradation of MO over Ag–Ag_2O/g-C_3N_4 photocatalyst under visible-light irradiation as follows. When under the visible-light exposure, both of the Ag_2O and g-C_3N_4 generate valence band holes (h^+) and conduction band electrons (e^-). In order to give a direct analysis, the potentials of the conduction band (CB) and valence band (VB) edges of Ag_2O and g-C_3N_4 were

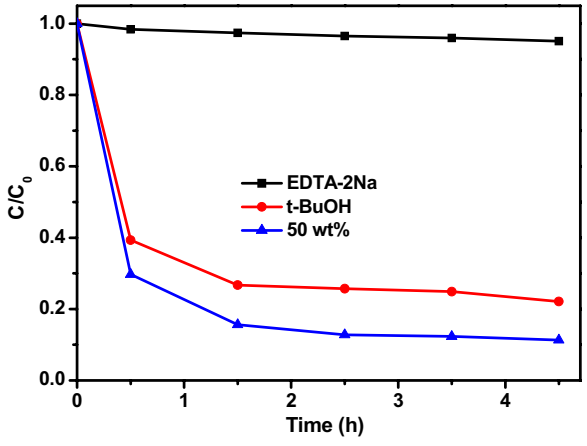

Fig. 8 Effect of different scavengers on the degradation of methyl orange in the presence of 50 wt% Ag–Ag_2O/g-C_3N_4 composites under visible light irradiation

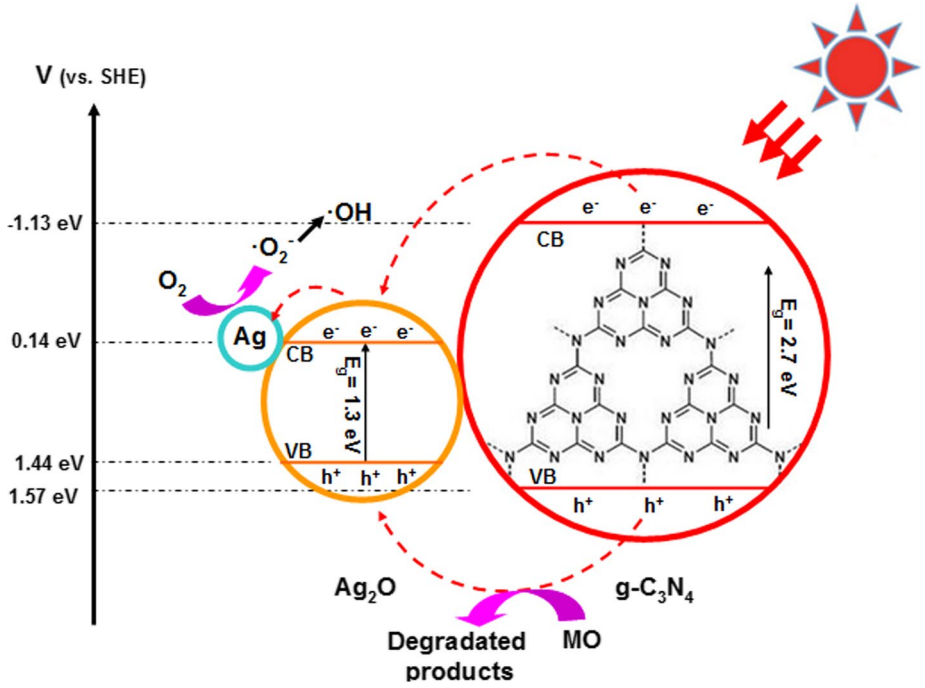

Fig. 9 Proposed mechanism for the promotion of the photocatalytic MO degradation performance of Ag–Ag_2O/g-C_3N_4 composites

evaluated by Mulliken electronegativity theory (Xu et al. 2013). Due to the valence band potential of Ag_2O was more negative than that of g-C_3N_4 and the conduction band potential of Ag_2O was more positive than that of g-C_3N_4, the photoinduced holes on the valence band and the electrons on the conduction band of g-C_3N_4 could move to Ag_2O.

In addition, the metallic Ag can further complete efficient electron migration process to efficiently inhibit the recombination of the photoexcited pairs (Xu et al. 2013). So it can be seen that even the VB and CB of g-C_3N_4 are higher than that of Ag_2O, the Ag can be worked as the charge transmission bridge, which transfers the photogenerated electrons from the CB of Ag_2O to Ag^0 and then the photogenerated electrons were trapped by O_2 to produce $\cdot O_2^-$. At last, the $\cdot O_2^-$ transformed into ·OH. As a result, with the assistance of Ag–Ag_2O, the Ag–Ag_2O/g-C_3N_4 photocatalysts could effectively enhance the separation of photoexcited electron-hole pairs and reduced the recombination of electrons and holes. Thus, the Ag–Ag_2O nanoparticles loaded on the surface of the g-C_3N_4 could form the heterojunction structure, which contributed to the promotion of the photocatalytic activity.

Conclusion

In summary, we have demonstrated that Ag–Ag_2O nanophases were active catalysts for degrading MO. The results revealed that the optimal activity of Ag–Ag_2O/g-C_3N_4 is 7.5 times as high as that of g-C_3N_4 and even better than that of Ag–Ag_2O. In this investigation the as-synthesized samples were characterized by a collection of techniques, such as XRD, SEM, TEM, HR-TEM, DRS, EDS, XPS and FT-IR. Based on structural analysis, we concluded that the Ag–Ag_2O nanoparticles are dispersed on the surface of the g-C_3N_4.

The modified g-C_3N_4 samples were robust and able to show better photocatalytic activities than Ag–Ag_2O and g-C_3N_4. In addition, the photocatalysis mechanism was also investigated by entrapping active species. These results indicated that the holes played important roles in the degradation of MO over sample Ag–Ag_2O/g-C_3N_4.

Additional file

Additional file 1. MO degradation by Ag-Ag_2O/g-C_3N_4 composites under visible-light irradiation.

Authors' contributions

XW prepared the sample, had done the experiment of the XRD, FT-IR, XPS, TEM, SEM, HR-TEM, DRS, transient photocurrent and MO dye degradation and drafted the manuscript. JY provided with design ideas and teaching methods to improve the article. HYJ, ZGC, YGX, LYH, QZ, YHS checked and improved the manuscript. HX conceived of the study, and participated in its design and coordination and helped to draft the manuscript. HML conceived of the study, and participated in its design and coordination and helped to draft the manuscript. All authors read and approved the final manuscript.

Author details

[1] School of Chemistry and Chemical Engineering, Institute for Energy Research, Jiangsu University, Zhenjiang 212013, People's Republic of China. [2] Hainan Provincial Key Lab of Fine Chemistry, Hainan University, Haikou 570228, Hainan, People's Republic of China. [3] School of Environmental and Chemical Engineering, Jiangsu University of Science and Technology, Zhenjiang 212003, People's Republic of China.

Acknowledgements

The authors genuinely appreciate the financial support of this work from the National Nature Science Foundation of China. The authors genuinely appreciate the financial support of this work by the National Nature Science Foundation of China (21476097, 21476098,21407065 and 21406094), the Natural Science Foundation of Jiangsu Province (BK20131207 and BK2012717, BK20140533).

Competing interests

All authors declare that they have no competing interests.

Received: 12 December 2015 Accepted: 12 February 2016
Published online: 24 March 2016

References

Cao SW, Yuan YP, Barber J, Loo SCJ, Xue C (2014) Noble-metal-free g-C_3N_4/Ni(dmgH)$_2$ composite for efficient photocatalytic hydrogen evolution under visible light irradiation. Appl Surf Sci 319:344–349

Chang F, Xie YC, Li CL, Chen J, Luo JR, Hu XF, Shen JW (2013) A facile modification of g-C_3N_4 with enhanced photocatalytic activity for degradation of methylene blue. Appl Surf Sci 280:967–974

Chang F, Zhang J, Xie YC, Chen J, Li CL, Wang J, Luo JR, Deng BQ, Hu XF (2014) Fabrication, characterization, and photocatalytic performance of exfoliated g-C_3N_4–TiO_2 hybrids. Appl Surf Sci 311:574–581

Chen W, Liu TY, Huang T, Liu XH, Zhu JW, Duan GR, Yang XJ (2015) In situ fabrication of novel Z-scheme Bi_2WO_6 quantum dots/g-C_3N_4 ultrathin nanosheets heterostructures with improved photocatalytic activity. Appl Surf Sci 355:379–387

Cho IS, Chen ZB, Forman AJ, Kim DR, Rao PM, Jaramillo TF, Zheng X (2011) Branched TiO_2 nanorods for photoelectrochemical hydrogen production. Nano Lett 11(11):4978–4984

Dong F, Li YH, Wang ZY, Ho WK (2015) Enhanced visible light photocatalytic activity and oxidation ability of porous graphene-like g-C_3N_4 nanosheets via thermal exfoliation. Appl Surf Sci 358:393–403

Huang LY, Xu H, Zhang RX, Cheng XN, Xia JX, Xu YG, Li HM (2013a) Synthesis and characterization of g-C_3N_4/MoO_3 photocatalyst with improved visible-light photoactivity. Appl Surf Sci 283:25–32

Huang LY, Xu H, Li YP, Li HM, Cheng XN, Xia JX, Xu YG, Cai GB (2013b) Visible-light-induced WO_3/g-C_3N_4 composites with enhanced photocatalytic activity. Dalton Trans 42(24):8606–8616

Li YB, Zhang HM, Liu PR, Wang D, Li Y, Zhao HJ (2013) Cross-linked g-C_3N_4/rGO nanocomposites with tunable band structure and enhanced visible light photocatalytic activity. Small 9(19):3336–3344

Li YF, Zhao Y, Fang L, Jin RX, Yang Y, Xing Y (2014) Highly efficient composite visible light-driven Ag–AgBr/g-C_3N_4 plasmonic photocatalyst for degrading organic pollutants. Mater Lett 126:5–8

Li ZJ, Wang JH, Zhu KX, Ma FL, Meng A (2015) Ag/g-C_3N_4 composite nanosheets: synthesis and enhanced visible photocatalytic activities. Nat Mater 145:167–170

Liu A, Cohen M (1989) Prediction of New low compressibility solids. Science 245(4920):841–842

Liu ZY, Zhang XT, Nishimoto S, Murakami T, Fujishima A (2008) Efficient photocatalytic degradation of gaseous acetaldehyde by highly ordered TiO_2 nanotube arrays. Environ Sci Technol 42(22):8547–8551

Liu CB, Cao CH, Luo XB, Luo SL (2015) Ag-bridged Ag_2O nanowire network/TiO_2 nanotube array p–n heterojunction as a highly efficient and stable visible light photocatalyst. J Hazard Mater 285:319–324

Lotsch BV, Schnick W (2006) From triazines to heptazines: novel nonmetal tricyanomelaminates as precursors for graphitic carbon nitride materials. Chem Mater 18(7):1891–1900
Melian EP, Díaza OG, Rodrigueza JMD, Colon G, Naviob JA, Macias M, Pena JP (2012) Effect of deposition of silver on structural characteristics and photoactivity of TiO_2-based Photocatalysts. Appl Catal B Environ 127:112–120
Min SX, Lu GX (2012) Enhanced electron transfer from the excited eosin Y to mpg-C_3N_4 for highly efficient hydrogen evolution under 550 nm irradiation. J Phys Chem C 116(37):19644–19652
Park JH, Kim S, Bard AJ (2006) Novel carbon-doped TiO_2 nanotube arrays with high aspect ratios for efficient solar water splitting. Nano Lett 6(1):24–28
Peng Y, Qin SC, Wang WS, Xu AW (2013) Fabrication of porous Cd-doped ZnO nanorods with enhanced photocatalytic activity and stability. CrystEngComm 15(33):6518–6525
Ren HT, Jia SY, Wu Y, Wu SH, Zhang TH, Han X (2014) Improved photochemical reactivities of Ag2O/g-C3N4 in phenol degradation under UV and visible light. Ind Eng Chem Res 53(45):17645–17653
Su FZ, Mathew SC, Lipner G, Fu XZ, Antonietti M, Blechert S, Wang XC (2010) mpg-C_3N_4-catalyzed selective oxidation of alcohols using O-2 and visible light. J Am Chem Soc 132(46):16299–16301
Subramanian V, Wolf E, Kamat PV (2001) Semiconductor-metal composite nanostructures. To what extent do metal nanoparticles improve the photocatalytic activity of TiO2 films. J Phys Chem B 105(46):11439–11446
Tian N, Huang HW, Guo YX, He Y, Zhang YH (2014) A g-C_3N_4/$Bi_2O_2CO_3$ composite with high visible-light-driven photocatalytic activity for rhodamine B degradation. Appl Surf Sci 322:249–254
Vignesh K, Kang M (2015) Facile synthesis, characterization and recyclable photocatalytic activity of Ag_2WO_4@g-C_3N_4. Mater Sci Eng B 199:30–36
Wang J, Zhang WD (2012) Modification of TiO_2 nanorod arrays by graphite-like C_3N_4 with high visible light photoelectrochemical activity. Electrochim Acta 71:10–16
Wang XC, Maeda K, Thomas A, Takanabe K, Xin G, Carlsson JM, Domen K, Antonietti M (2009a) A metal-free polymeric photocatalyst for hydrogen production from water under visible light. Nat Mater 8(1):76–80
Wang XC, Maeda K, Chen XF, Takanabe K, Domen K, Hou YD, Fu XZ, Antonietti M (2009b) Polymer semiconductors for artificial photosynthesis: hydrogen evolution by mesoporous graphitic carbon nitride with visible light. J Am Chem Soc 131(5):1680
Wang XF, Li SF, Yu HG, Yu JG, Liu SW (2011) Ag_2O as a new visible-light photocatalyst: self-stability and high photocatalytic activity. Chem Eur J 17(28):7777–7780
Wang SM, Li DL, Sun C, Yang SG, Guan Y, He H (2014) Synthesis and characterization of g-C_3N_4/Ag_3VO_4 composites with significantly enhanced visible-light photocatalytic activity for triphenylmethane dye degradation. Appl Catal B Environ 144:885–892
Xie Y, Kum J, Zhao XJ, Cho SO (2011) Enhanced photocatalytic activity of mesoporous S–N-codoped TiO_2 loaded with Ag nanoparticles. Semicond Sci Technol 26(8):085037
Xiu ZL, Bo H, Wu YZ, Hao XP (2014) Graphite-like C_3N_4 modified Ag_3PO_4 nanoparticles with highly enhanced photocatalytic activities under visible light irradiation. Appl Surf Sci 289:394–399
Xu H, Li HM, Xia JX, Yin S, Luo ZJ, Liu L, Xu L (2011) One-pot synthesis of visible-light-driven plasmonic photocatalyst Ag/AgCl in ionic liquid. ACS Appl Mater Interfaces 3(1):22–29
Xu M, Han L, Dong SJ (2013a) Facile fabrication of highly efficient g-C_3N_4/Ag_2O heterostructured photocatalysts with enhanced visible-light photocatalytic activity. ACS Appl Mater Interfaces 5(23):12533–12540
Xu H, Yan J, Xu YG, Song YH, Li HM, Xia JX, Huang CJ, Wan HL (2013b) Novel visible-light-driven AgX/graphite-like C_3N_4 (X=Br, I) hybrid materials with synergistic photocatalytic activity. Appl Catal B Environ 129:182–193
Yan SC, Li ZS, Zou ZG (2010) Photodegradation of rhodamine B and methyl orange over boron-doped g-C_3N_4 under visible light irradiation. Langmuir 26(6):3894–3901
Yan HJ, Chen Y, Xu SM (2012) Synthesis of graphitic carbon nitride by directly heating sulfuric acid treated melamine for enhanced photocatalytic H-2 production from water under visible light. Int J Hydrogen Energy 37(1):125–133
Yan J, Xu H, Xu YG, Wang C, Song YH, Xia JX, Li HM (2014) Synthesis, characterization and photocatalytic activity of Ag/AgCl/Graphite-Like C_3N_4 under visible light irradiation. J Nanosci Nanotechnol 14(9):6809–6815
Yang XY, Wolcott A, Wang GM, Sobo A, Fitzmorris RC, Qian F, Zhang JZ, Li Y (2009) Nitrogen-doped ZnO nanowire arrays for photoelectrochemical water splitting. Nano Lett 9(6):2331–2336
Yao XX, Liu XH, Hu XL (2014) Synthesis of the Ag/AgCl/g-C_3N_4 composite with high photocatalytic activity under visible light irradiation. Chemcatchem 6(12):3409–3418
Yu JG, Xiong JF, Cheng B, Liu SW (2005) Fabrication and characterization of Ag–TiO_2 multiphase nanocomposite thin films with enhanced photocatalytic activity. Appl Catal B Environ 60(3–4):211–221
Yu HG, Liu R, Wang XF, Wang P, Yu JG (2012) Enhanced visible-light photocatalytic activity of Bi_2WO_6 nanoparticles by Ag_2O cocatalyst. Appl Catal B Environ 111:326–333
Yu CL, Li G, Kumar S, Yang K, Jin RC (2014) Phase transformation synthesis of novel Ag_2O/Ag_2CO_3 heterostructures with high visible light efficiency in photocatalytic degradation of pollutants. Adv Mater 26(6):892–898
Yu HG, Chen FY, Chen F, Wang XF (2015) In situ self-transformation synthesis of g-C_3N_4-modified CdS heterostructure with enhanced photocatalytic activity. Appl Surf Sci 358:385–392
Zhao SS, Chen S, Yu HT, Quan X (2012) g-C_3N_4/TiO_2 hybrid photocatalyst with wide absorption wavelength range and effective photogenerated charge separation. Sep Purif Technol 99:50–54
Zhao W, Guo Y, Wang SM, He H, Sun C, Yang SG (2015) A novel ternary plasmonic photocatalyst: ultrathin g-C_3N_4 nanosheet hybrided by Ag/$AgVO_3$ nanoribbons with enhanced visible-light photocatalytic performance. Appl Catal B Environ 165:335–343
Zhou WJ, Liu H, Wang JY, Liu D, Du GJ, Cui JJ (2010) Ag_2O/TiO_2 nanobelts heterostructure with enhanced ultraviolet and visible photocatalytic activity. ACS Appl Mater Interfaces 2(8):2385–2392
Zong X, Sun CH, Yu H, Chen ZG, Xing Z, Ye DL, Lu GQ, Li XY, Wang LZ (2013) Activation of photocatalytic water oxidation on N-doped ZnO bundle-like nanoparticles under visible light. J Phys Chem C 117(10):4937–4942